ILASS 2008
Sep. 8-10, 2008, Como Lake, Italy

Paper ID ILASS08-1-15

LIQUID SHEET DISINTEGRATION AT HIGH PRESSURE

Vital G Fernández*, P. Berthoumieu*, G. Lavergne*

*ONERA (Office National d'Études et de la Recherche Aérospatiales)
Heterogeneous, Multiphase Flows Unit
Aerodynamic and Energetic Models Department
BP 4025, avenue Edouard Belin, 31055 Toulouse cedex 4, France

Vital.Gutierrez_Fernandez@onecert.fr

ABSTRACT
The behaviour of the primary atomization has been analyzed in the laboratory LACOM at the ONERA Fauga-Mauzac. The techniques, employed to this aim, included fast camera visualization, Laser reflexion intensity and LDV. The air flow pressure was increased from the atmospheric conditions to 6 bars absolute pressure. The air velocity was kept constant for each back pressure by increasing the air mass flow. An airblast atomizer generated a thin planar liquid sheet of 300 µm thickness. The atomization mechanisms, described in the bibliography, were observed in these environments, as long as, the momentum flux ratio would remain constant. The variables measured were the global oscillation frequency, break-up distance and separation between ligaments. Atmospheric empirical formulations, for these variables, were updated to obtain convergence of the trendlines, as the air density augmented.

INTRODUCTION

Nowadays, the combustion processes weight heavily in the scientific community, both for ecological and economical reasons. In a combustion chamber, the phenomena which disintegrate the continuous liquid flow into droplets, it is known as primary atomization. The aim of this experimental research was to observe the primary atomization at operating pressure conditions, close to those of a turbine combustion process.

In turbine engines, the fuel injection is usually accomplished via an airblast atomizer. This is due to its greater efficiency at generating small droplets in continuous-flow systems, with relative low air velocities [1]. At the ONERA Toulouse scientific investigations, in the experimental, theoretical and numerical domains, have been oriented towards the liquid disintegration, provided by these atomizers. This kind of injectors generates a thin liquid sheet, which oscillates by the action of two parallel air flows. As the liquid sheet is energized, by the air flows, longitudinal and transversal instabilities arise and disintegrate it, into droplets.

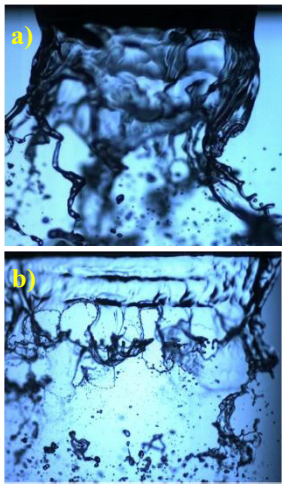

Fig.1: Airblast Liquid sheet:
v_{water} = 1m/s, v_{air} = 30m/s
a) Annular b) Planar

Real designs have favoured annular, geometries, Fig.1a. However, many cases, experimental and numerical studies have been performed in a planar configuration, Fig.1b. This choice lied on its simpler design and adaptability to optical techniques. Furthermore, experimental and numerical evidence has confirmed, a homogeneous behaviour, between both geometries [2], [3]. This similarity holds true for annular injectors, with a diameter greater than 1 cm, as smaller airblast injectors behaved as liquid jets [4].

The references included in this article lead to remarkable experimental studies of the primary atomization, at atmospheric conditions. Nevertheless, to the best authors' knowledge, insufficient tests have been performed at the real operating conditions of a turbine engine [5], [6]. Reaching this point, it was necessary to validate the available empirical formulas, at increased pressure environments. In order to determine, whether, it would be sufficient to change the magnitude of the air density, or if, the dynamic behaviour of the primary atomization would vary. In the latter case, it would be required to update these available relations.

The fluid flows of the experimental activity hereby presented were described by the following dimensionless parameters: A gas Reynolds number, which ranged from a transitional value of 1.2×10^5 to a turbulent magnitude of 2.5×10^6 . The tested liquid was water, whose Reynolds number went from 150 to 600. The characteristic length for the Re_{Air} was the injectors cord, whereas for the Re_{Water}, the liquid sheet thickness was employed. The Webber number had a valued as low as 1.8 and up to 142, where its characteristic length was again the injector's cord. Finally, the momentum flux ratio, M, increased from 0.5 to 35.5.

Regarding the injector's geometry: It had a NACA 63-010 profile, a cord length of 89 mm. It generated a thin liquid sheet of 40 mm width and was 300 µm thickness. Ultimately, the injector's lips had a thickness of 690 µm

In the following sections, this article includes a brief description of the experimental facilities. Immediately afterwards and a discussion of the results is presented in two parts: a qualitative study of the atomization mechanisms and the quantitative results on three liquid sheet variables: the global oscillation frequency, break up length and separation between ligaments. Finally a set of conclusions is presented.

EXPERIMENTAL SET UP AND PROCEDURE

Flow Conditions

One of the reasons behind the complexity of the primary atomization field lies on the number of variables, which affect its behaviour. The most fundamental comparisons have been done at different liquid and air velocities or at different inner outer fluid velocities [7]. Once this has been done, researchers have opted to vary the liquid sheet thickness, and/or the cross sectional area of the air flow outlet [8]. By all means, tests have been performed with diverse liquids [9].

A very exhaustive set of studies was performed by Mansour and Chigier [10], which enabled the characterisation of the liquid sheet disintegration via the liquid velocity, gas velocity and the global oscillation frequency. This research lied inside the threshold of their investigation. The air velocity, varied from 20 m/s to 70 m/s, for liquid velocities of 1 and 2 m/s. The innovation of this research consisted in increasing the back pressure from the atmospheric values up to 6 bars absolute pressure. This is a modest pressure value compared to the 10 bars in helicopter or the 40 bars in aeroplane turbine engines. Regardless, it provided a valuable insight of the planar liquid sheet behaviour.

A final set of measurements was carried out at atmospheric conditions with a liquid velocity of 0.5 m/s. This was done in order to obtain an increment in magnitude of the momentum flux ratio without increasing the air flow pressure. All these measurements were done in water.

Experimental equipment

The sketch, on Fig.2**,** shows the injection line employed in this investigation. After the pipe's elbow, the air stream went through a screen and a tube length 30 times the equivalent diameter; before it flowed around the injector. The duct had an internal square section with a 46 mm edge. In addition a square tube with optical openings was installed after the airblast atomizer. The air flow pressure in the vessel was varied by modifying the incoming flow conditions and using the valve at the end of the injection line.

It is worth mentioning that initially, the installation was designed to measure the air velocity via a sonic throat technique. However, the natural vibration of the facility, due to flow through a sonic throat had a considerable effect, on the liquid sheet behaviour. The oscillations observed on the liquid sheet, Fig.3, had wavelength of the same order as those predicted by the empirical research of Lalo [11]. Her formula was aimed to determine the wavelengths on a droplet subjected to a piezoelectric vibrator.

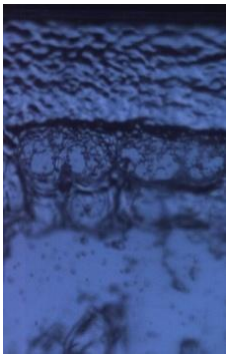

Fig.3: Liquid Sheet under the effect of sonic throat vibration

The solution of this eventuality involved the replacement of the sonic throat and designing an averaging pitot tube with a 5 holes T-chebycheff distribution. The calibration performed via a LDV system (Laser Doppler Velocimetry) confirmed its accuracy at all pressure conditions.

The pieces of equipment employed in this experimental study may also be observed in Fig.2.These consisted in:

a) A Fast Camera Model Phantom.9: as with any fast camera, there was a compromise between image size and acquisition rate. Consequently, it was decided to take two sets of visualizations at each flow condition. The first one with images of 584×800 pixels (10×17 mm) size recorded at 3000 Hz, to measure space dependable variables, such as, the break up length or separation between ligaments. The second one, with images of 368×600 pixels (6x10 mm) size recorded at 6000 Hz, to measure time dependable variables, like ligaments diameter or length. In order to obtain the magnitude of these variables, it was required to apply a post imaging process.

b) Laser Diode: in combination with a photoreceptor was used to measure the global oscillation frequency, via a Laser reflexion intensity oscillation technique: The intensity signal of the reflected beam was treated by a Fast Fourier Transform. In these measurements the laser was place at an angle with respect the injection plane vector, as showed in Fig.2

c) LDV: This instrument was employed to characterise the air flow boundary layer, at the injector outlet. This was accomplished by determining the velocity profile along the y direction. Unfortunately, due to technical contingencies, it was unattainable to perform measurements, at a distance closer than 0.2 mm.

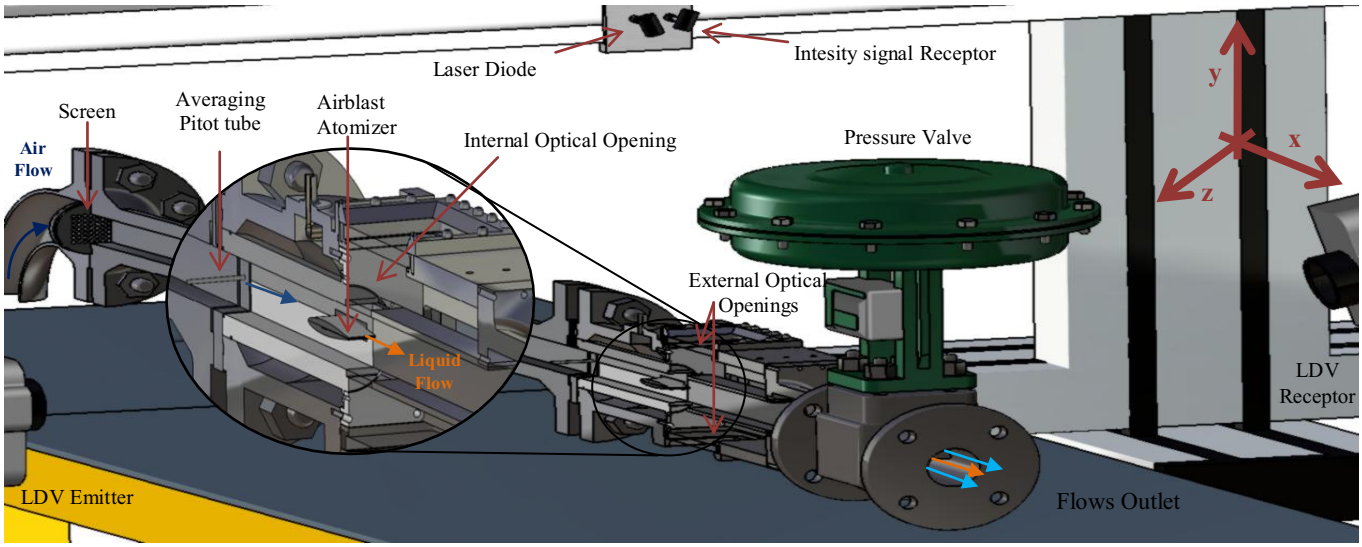

Fig.2: Injection Line Sketch. Detail airblast atomizer

QUALITATIVE RESULTS

The application of a fast camera enabled the visualization of the primary atomization to a great detail. At this level, it was possible to make a distinction between the diverse *liquid deformations* and *atomization mechanisms*. The former term includes the different shapes observed, when a liquid is submitted to aerodynamic forces. A few examples of these shapes included the shaping of a liquid into a flat surface (membrane), into a thin cylinder (ligament), into a low circularity sphere (bulgy droplet)... The latter expression, *atomization mechanisms*, referred to a combination of liquid deformations originated by a set of fluid instabilities, which disintegrate the continuous liquid flow into droplets.

It has been found that the appearance of each atomization mechanisms may be simply predicted by the magnitude of the air to liquid momentum ratio:

$$M_x = \frac{\rho_g v_g^2 e_g}{\rho_l v_l^2 e_l} \qquad (1)$$

Where the suffixes (g) and (l) refer to the gas and liquid phases respectively. The parameters $e_{g,l}$ is a characteristic length of the injector gas and liquid phase geometries. In this research e_g/e_n equalled 153, the ratio of the duct edge length by liquid sheet thickness.

On the other hand, many researchers have favoured a simplification, which has become the most established nondimensional parameter. This is the momentum flux ratio:

$$M = \frac{\rho_g v_g^2}{\rho_l v_l^2} \qquad (2)$$

In this research, this momentum flux ratio varied from 0.5 to 35.5.

Stretched ligament Break up

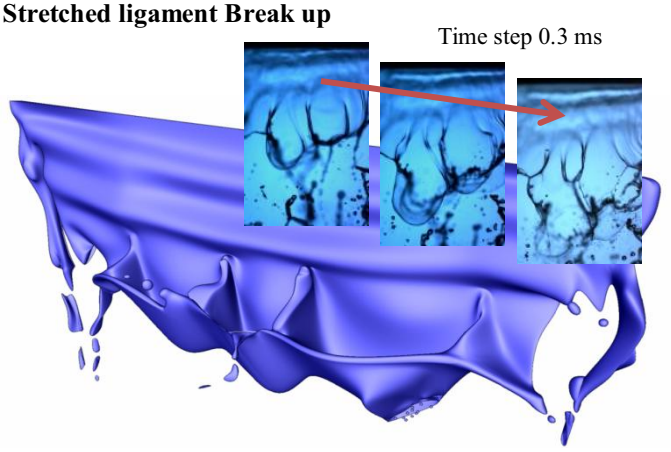

Fig.4: Sketch of Stretched ligament break-up. Detail sack formation

The first atomization mechanism observed, was predominant for values of the momentum flux ratio from 1 to 8. This atomization mechanism was named Stretched Ligament Break-up by Stapper and Samuelsen, [12]. This name was motivated, by the liquid deformation of long longitudinal fingers, which are characteristic in this regime

Three droplets sources could be distinguished, according to the droplet size.

a) The first case, to which the smallest droplets belonged, was the perforation of big bag-like structures, which formed at the end of the continuous liquid region. This liquid deformation was similar to the droplet *bag break-up* [13] in the secondary atomization. Indeed, for this range for the momentum flux ratio, the values of the We (0.50-17) and Re_{Air} (1.2×10^5 and 4.1×10^5) guaranteed a dome shaped membrane break up. The length and number of droplets were inversely proportional to the size of the dynamic pressure ratio. The visualizations performed pointed out that the length of these bag-like structures, and hence, that of the longitudinal ligaments, was of the same order than the continuous liquid region.

b) The second one, which generated medium size droplets, corresponded to the disintegration of the longitudinal ligaments. Once the bag-like structures had collapsed, the remaining membranes shrank into streamwise rims. This shirking occurred, while still shedding droplets. These rims became the longitudinal ligaments. The diameter of these ligaments was never superior to 500 µm. Their disintegration corresponded to the Rayleigh instability.

c) The largest droplets were generated via the break-up of the transversal ligaments. These rims were the crests of the longitudinal waves. At relative low momentum flux ratio, below 5, (60 m/s at atmospheric conditions), the droplets formed had a high circularity, with a diameter up to 1.5 mm. At higher air velocities; however, the bag like structures did not have the time to collapse before the transversal ligaments did. At this point, the transversal ligaments broke in the shape of "jellyfish", as, transversal structure remained attached to the streamwise ligaments.

This atomization mechanism has also been named, Sinusoidal mode by Mansour and Chigier [14]. This is because of the oscillations observed on the liquid film. This dynamic behaviour may be explained by the fluids subjected to the Kelvin-Helmholtz instability. Furthermore, this oscillation determined the length of the streamwise ligaments and the diameter of the transversal ligaments.

Cellular Break up:

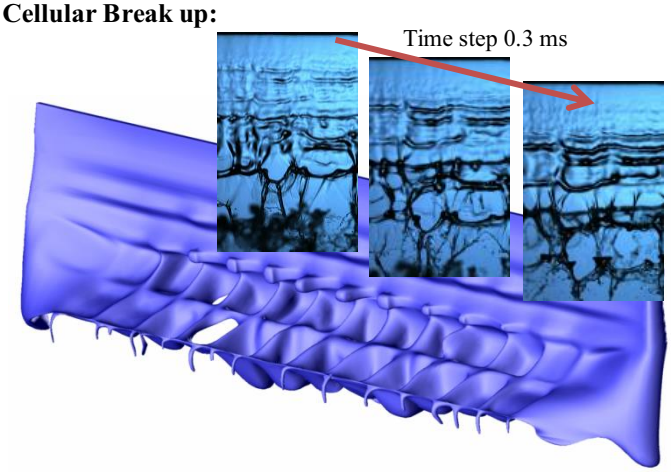

Fig.5: Sketch Cellular Break-up. Detail transversal ligaments

For the lowest values of the momentum flux ratio, below 0.50, the atomization mechanism known as cellular break-up arose [12]. It was the regime corresponding to high values for the liquid dynamic pressure. The reasoning behind this name was the formation of multiple lines and columns of liquid membranes limited by longitudinal and transversal liquid rims.

In this regime, it was still possible to organize the generation of droplet formation into bag-like, longitudinal and

transversal ligaments. Nonetheless, the prevalence of the liquid deformations differed with the previous atomization mechanism:

a) The smallest droplets were generated by the collapse of bag-like structures. In this regime, though, there were multiple lines of sacks. Up to 2 lines and 7 columns for a liquid velocity of 2m/s were observed in this research. These bag-like structures were smaller than in the previous regime, and hence, generate a smaller number of droplets during the puncturing process.
b) Medium size droplets were produced by the break-up of the longitudinal ligament via the Rayleigh instability. Comparing with the previous regime, since multiple columns of membranes were formed, the population of ligaments increased. Conversely, these liquid fingers were shorter. The diameter of the streamwise ligaments was of the same magnitude as in the stretched ligament breakup.
c) Experimental observations have established proportionality between the droplet size and the liquid velocity [15]. This was due to the fact that in this regime the atomization of transversal ligaments had a greater predominance. Moreover, as it can be observed in Fig.5, in this mechanism the transversal ligaments are formed before the rupture of the membranes. The size of droplets generated in this mechanism reached the 2mm.

As the previous mechanism, the cellular break-up was also analysed by Mansour and Chigier, who named it dilational mode. This was due to the type longitudinal oscillation found. The raise in liquid velocity translated into greater break-up distances. Under these circumstances the transversal oscillation affected the liquid sheet for a longer time, generating several lines of "liquid cells". On the other hand, the crests of the longitudinal waves were deformed by the action of the Rayleigh-Plateau instability. It was this transversal instability, which determined the separation of the longitudinal ligaments and the diameter of the transversal ligaments.

Wavy Regime:

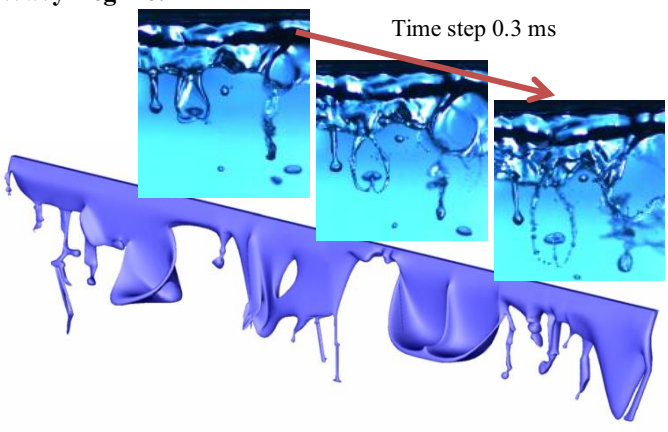

Fig.6: Sketch Wavy Break up. Detail longitudinal ligaments

The final regime visualized, within the flow conditions tested, was named as Wavy regime, by Fraser and Eisenklam [16]. This regime took place at the highest values of the momentum flux ratio, above 8. It was hence, the regime which became predominant, once the back pressure increased in magnitude. Furthermore, this atomization mechanism appeared, once the water injection velocity was reduced to 0.5 m/s at atmospheric conditions.

The instabilities, which provided the disintegration, were a consequence of the turbulent flows. Under these conditions, local deformations on the film surface created bulges and protuberances. Unlike the previous atomization mechanisms neither uniform spatial, nor temporal pattern could be distinguished in the water disintegration. In any case, it may be possible to classify the means, in which the continuous liquid region fragmented into droplets:

a) The scaled sketch on Fig.6, shows how this regime was characterised by the formation of highly irregular shaped longitudinal ligaments. These streamwise ligaments were longer and thicker than their counterparts at lower values for the momentum flux ratio. The rupture of these structures into droplets was not strictly ruled by the Rayleigh instability. Since, the majority of the streamwise structures were torn away before the instability could propagate.
b) The disintegration of sacks into a shower of very fine drops still occurred. However, these liquid deformations took place randomly. Moreover, these did not only form in the continuous liquid region but also in the longitudinal ligaments. In the later case, as the bag like structure collapsed, extra liquid fingers formed, contributing to the final ligaments shape.
c) Finally, at the highest values of M, the continuous liquid region was eventually torn away in the form of big bulgy droplets. These were due to the fact, that the longitudinal wave did not have time to developed: Since no transversal ligament was formed, any perforation of the continuous region propagated inevitably wind down.

QUANTITATIVE RESULTS AND DISCUSSION

In the bibliography, it is possible to find several relations to characterise the different variables, which described the liquid sheet. In the presented paper, we included the results corresponding to measurements on the global oscillation frequency, the break-up length and the separation between ligaments. Larricq [17] provided three empirical relations for these variables. As the value of the back pressure increased, it was possible to observe the robustness of the equations. In the first two cases, the equations did not longer hold true, hence, they were updated.

Global Oscillation Frequency

Once the liquid sheet was injected within an air flow stream, it was bound to suffer a perturbation. The surface tension forces would damp this perturbation, and hence, deform-back the protuberance. However, at this point the air flow experienced a local increase in the static pressure, as the local velocity decreased close to the protuberance. Therefore, the aerodynamic forces acted as a unstable mechanism from a critical value of the air velocity.

This phenomenon is known as the Kelvin-Helmholtz instability. It occurs at concurrent fluid flows with different magnitudes in density and velocity. The variable named global oscillation frequency referred to the wave generated by this fluids instability.

In Fig.7, the magnitude of the Global Oscillation Frequency has been plotted versus the air velocity. These values corresponded to both liquid velocity and all tested back pressures. As expected, from past experience, the relation between the oscillation frequency and the air pressure could

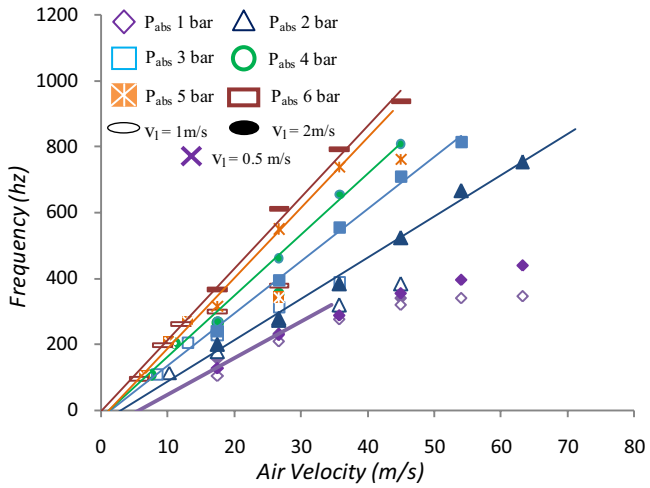

Fig.7: Global Oscillation Frequency versus Air Velocity

be approximated by a logarithmic trendline. The liquid velocity had a weaker effect on the oscillation frequency than the air velocity. Nevertheless, as it may be observed on the graph, an increase in the liquid flow translated into an increment of the higher gradient region, delaying the lowest gradient zone.

It was observed that an increment of the back pressure translated into a rise of the oscillation frequency for both regions. It is concluded that as the energy per unit volume increased so did the energy transfer rate to the liquid flow. It should be noticed, that the global oscillation frequency showed the same logarithm behaviour, for every atomization mechanisms, at all the flow conditions tested. However, as the momentum flux ratio increased, stepping deeper into the wavy regime, the measurements became less obvious. The noise generated by the other liquid instabilities hindered the observation of any dominant frequency.

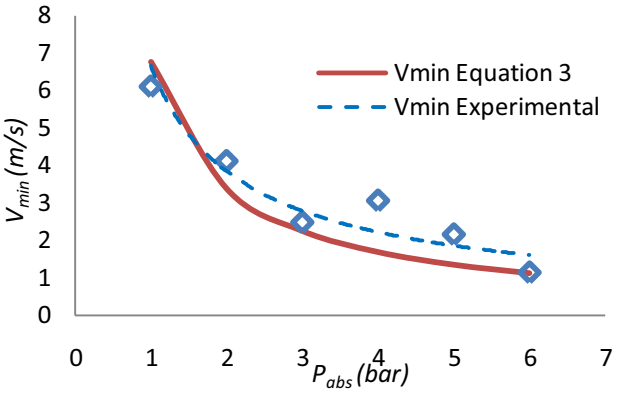

Fig.8: Minimum air velocity versus Back pressure

As it was showed by Lozano [18], there was a minimum air velocity, for which the longitudinal oscillation occurred. In these set of experiences, we measured a smaller value for this parameter than the 9 m/s Lozano obtained. This parameter has been found to vary with the liquid (with values below 3 m/s for ethanol and kerosene) but to remain independent of the liquid velocity. In order to determine this parameter, in Fig.7, it may be observed, how the values in the highest gradient region at both liquid velocities formed a linear trendline. The point at which these trendlines cut the horizontal axis marked the magnitude of the minimum air velocity. Confirming previous hypothesis, this parameter was inversely proportional to the air flow pressure. In Fig.8, the value of the minimum velocity was plotted versus the back pressure.

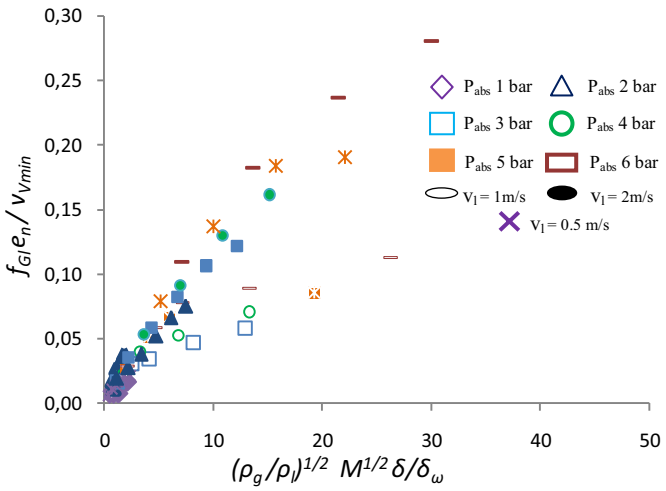

Fig.9: Global Oscillation Frequency, adimensional format

The following equation, supported by the experimental results, was found convenient to predict the value of the minimum air velocity. The trendline of this equation has been plotted as well in Fig.8:

$$V_{min} = \frac{\sigma_l}{\mu_l}\frac{\rho_l}{\rho_g} 10^{-5} \qquad (3)$$

As predicted by the Kelvin-Helmholtz instability theory: This minimum air velocity is proportional to the surface tension of the fluid, which damped the oscillation and inversely proportional to the dynamic viscosity, which enhances the energy transfer. Furthermore, it might explain the difference between the value of Lozano and the one calculated in this research: In the case of water, a variation of 10 degrees in temperature could considerably affect the magnitude of the dynamic viscosity, which would affect the final value of V_{min}.

Following the example of Larricq, we attempted a dimensional analysis on the results based on past experience. The description of oscillating flow mechanisms, in a dimensionless format, is commonly accomplished by means of the Strouhal number:

$$Str = \frac{f_{Gl} e_l}{V_{min}} \qquad (4)$$

It may be studied in Fig.9; the dimensionless form of the global oscillation frequency could be expressed as a function of the density ratio, the momentum flux ratio and the ratio of the boundary layer with the vorticity thickness.

$$\frac{f_{Gl} e_l}{V_{min}} = \left(\frac{\rho_l}{\rho_g}\right)^{1/2} M^{1/2} \frac{\delta}{\delta_\omega} \qquad (5)$$

The vorticity thickness has been found to provide a right measure of the boundary layer behaviour in two phase flows. This ratio was defined as:

$$\delta_\omega = \frac{v_g - v_l}{\left(\frac{dv_g}{dy}\right)_{wall}} \qquad (6)$$

The technical limitation of the LDV system rendered the possibility of measuring the flow velocity at a distance closer than 0.2 mm, unavailable. In order to determine the value of the wall velocity gradient a theoretical approach was chosen:

$$\left(\frac{dv_g}{dy}\right)_{wall} = \frac{1}{\mu_g} C_{f,c_{inj}} {}^{1}/_{2}\rho_g v_g^2 = \frac{{}^{1}/_{2} k_f \rho_g v_g^2}{\mu_g Re_{c_{inj}}^{1/5}} \qquad (7)$$

Where, k_f is a empirical factor with a value of 0.059 [19].

Break-Up Length

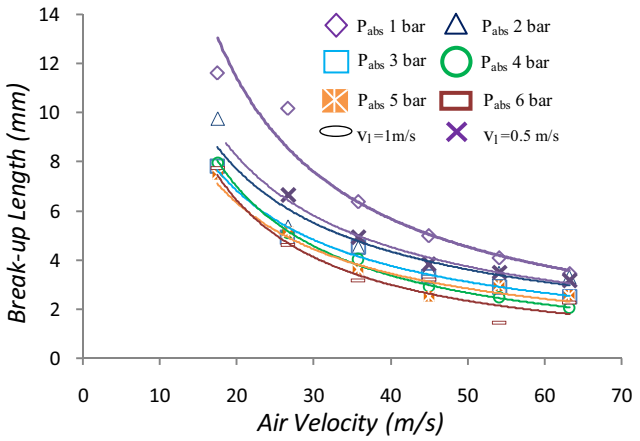

Fig.10: Break-up Length versus Air Velocity, v_l = 1 m/s

The break up length has been defined as the distance from the injector outlet to the end of the continuous liquid region. This variable has a considerable influence in the final spray penetration. In the case of the stretched ligament break-up and the cellular break-up, the measurement of this length was straight forward, at all times. Conversely, in the case of the wavy atomization mechanism, this length was not so easily calculated, from the visualizations. In order to guarantee the homogeneity of the results at all atomization mechanisms; the break-up length measured in this regime was established as the distance from the injector outlet, to the streamwise ligaments formation.

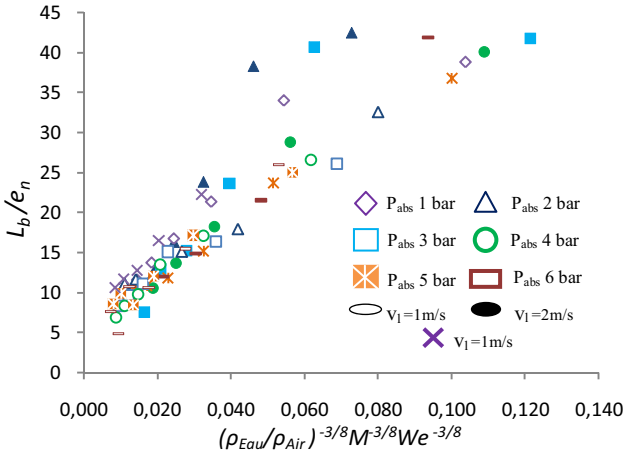

Fig.11: Break-up Length adimensional format

In Fig.10, the break-up length was plotted versus the air velocity for each tested back pressure. It may be gleaned how this length is proportional to the liquid dynamic pressure and inversely proportional to gas one. This was consistent with the measurements of the global oscillation frequency and the dynamic behaviour of the liquid sheet. As the liquid sheet was energised at a greater rate, it broke-up closer to the injector.

Performing a dimensional analysis, it was learned that at all tested operating conditions, the break-up length was a function of the density ratio, the momentum flux ratio and the Weber number. In the latter dimensionless ratio, the liquid sheet thickness was set as characteristic length:

$$\frac{L_b}{e} = \left(\frac{\rho_g}{\rho_l}\right)^{3/8} M^{-3/8} We_\delta^{-3/8} \qquad (8)$$

The graph plotted in Fig.11, showed the data measured at the six air velocities, two liquid velocities and six back pressures. It may be observed that for the lowest values of the relative velocity the points did not fit the trendline. This might be explained by the fact that for these points, the liquid edges of a planar geometry, still formed an angle injection, and hence, they tended to stabilize the liquid oscillation.

Separation between Ligaments

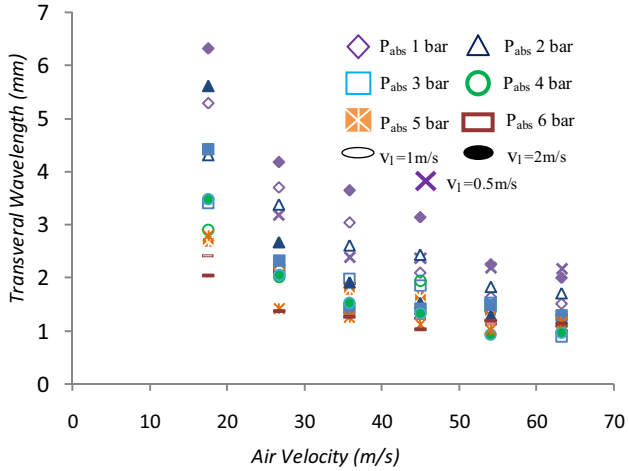

Fig.12: Transversal wavelength versus Air Velocity

In determining the droplet generation rate, the separation between ligaments is a critical factor. Furthermore, Marmottant [20] showed the strong relation between this length and the droplets diameter. This distance corresponds to the wavelength of the transversal instability.

This transversal oscillation has been dynamically described by the Rayleigh-Plateau instability. The crests of the liquid sheet generated by this motion may be approximated to a falling cylinder. Contrasting the previous instability, the surface tension contributed to deform the liquid sheet, as the liquid tended to distribute its volume to reduce the surface area to a minimum.

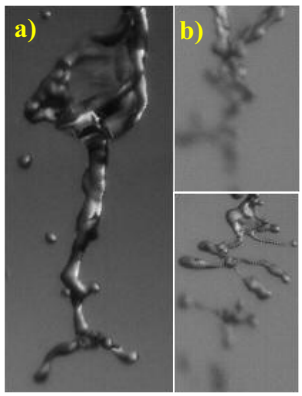

Fig.13: Wavy Regime:
a) Big ligament subjected to sack formation
b) Collision of two small ligaments

In the previous graph, Fig.12, the transversal wavelength has been plotted versus the air speed for all tested conditions. An initial observation confirmed the principles of the Rayleigh instability, by which, this wavelength was inversely proportional to the air flow velocity. Nevertheless, a more careful observation revealed a lack in homogeneity. A consequence of plotting results from different atomization mechanisms. It is the case of a liquid flow of 2 m/s at atmospheric conditions, for which the lowest

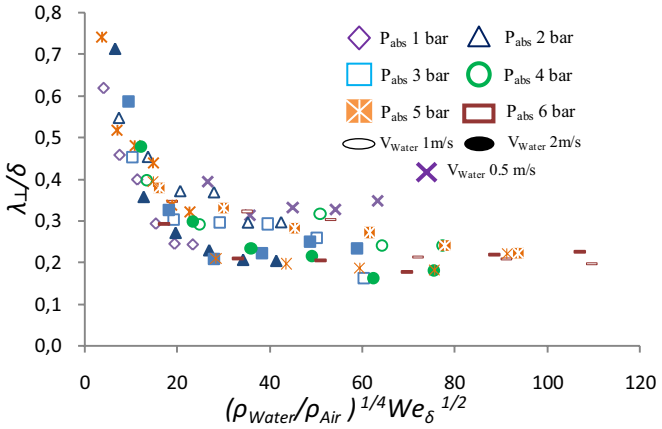

Fig.14: Separation between ligaments, adimensional format

transversal wavelength were found. In this zone cellular break-up became predominant, which had lower values of the separation between ligaments than the stretched ligament break-up.

In contrast, as the air dynamic pressure increased and the wavy regime became predominant, the distance between ligaments decreased to a minimum. The visualizations of the wavy atomization mechanism showed the behaviour of the longitudinal ligaments. These were not uniformly generated nor in space nor in time. Since the position of the ligaments was measured in a time basis, consecutive ligaments could not always be captured. A consequence of these "missing ligaments" was found in averaging of the data. At all tested flow conditions, the smaller wavelength, which could be determined was 1mm.

Moreover, as it may be observed in Fig.13, the definition of a ligament in this regime was very subjective. Complex ligament shapes were the result of the collision between ligaments or the formation of bag-like structures at the beginning and the end of the liquid fingers.

The dimensional analysis of the measurements performed, generated the chart in Fig.14. This graph is based in on the empiric relation of Larricq:

$$\frac{\lambda_{\perp}}{\delta} = \left(\frac{\rho_g}{\rho_l}\right)^{1/4} We_{\delta}^{1/2} \qquad (8)$$

Where the characteristic length of the Weber number is the boundary layer thickness.

A careful examination of this graph taught us that for a water velocity of 2 m/s, this equation was valid at increasing pressure conditions. This corresponded to intermediate values of the momentum flux ratio. However, as M increased the data points started to diverge. This was the point, at which the wavy regime became predominant

CONCLUSIONS

A modest increased in the air flow back pressure provided a valuable insight in the primary atomization phenomenon. It has been confirmed that the momentum flux ratio may be employed to predict the appearance of the diverse atomization mechanisms: the wavy regime occurred in high dynamic pressure environments and at atmospheric conditions with a low liquid dynamic pressure.

The minimum air velocity, at which the global oscillation frequency occurred, was determined for six back pressure values, in water. Once this data was compiled, it was possible to derive an empirical relation based on the gas and liquid physical properties. The next step in the confirmation of this equation will require further measurements of the global oscillation frequency, in additional liquids.

The authors have found that the fact of having a qualitative insight of the diverse atomization mechanisms and liquid deformations was essential if a homogenous relation, at all operating conditions, was desired.

For the three variables hereby presented, it may be concluded:

1. The global oscillation frequency had its magnitude increased with the raise in back pressure. Still, it showed the same logarithmic behaviour at all tested back pressures and every regime. The exception, however, lied in the highest value of M were the signal noise hindered the measurements.
2. The break-up length in the wavy regime was established as the length from the injector exit to the formation of a longitudinal ligament. Under this assumption the variable showed the same behaviour as at atmospheric conditions. As expected its value was inversely proportional to the gas density
3. A time basis measurement on the separation between ligaments was accomplished. A dimensional analysis showed that the correlation of Larricq, at atmospheric conditions, was valid for the stretched ligament break-up and cellular break-up at increasing pressure. However, in the wavy regime the data did not fit in correlation. This was due to the fact that consecutive ligaments did not formed uniformly in time. Therefore, once the results were averaged a greater value for the transversal wavelength than expected, was found. Overall, the transversal wavelength decreased with the back pressure.

FUTURE WORK

In the short term, the recorded visualizations will be employed to measure additional variables such as the ligaments length and diameter.

Once this medium term, new measurements will be accomplished at increasing pressure conditions and a different fluid flow; likely tests will be repeated with kerosene.

On the longer term, once the whole research plan is complete, it is expected to obtain a complete data base of the liquid sheet. The aim of this data base is to provided support to DNS (Direct Numerical Simulation) studies.

ACKNOWLEDGMENT

The authors wish to thank each other for work accomplished together.

As always, the worked performed by the staff at the ONERA Fauga-Mauzac LACOM facility was inestimable.

NOMENCLATURE

Symbol	Quantity	SI Unit
c_{inj}	Airblast Cord Length	m
e_l	Liquid sheet thickness	m
e_g	Air duct side length	m
f_{Gl}	Global Oscillation Frequency	hz
$k_f = 0.059$	Friction coefficient constant	
v_g	Gas Velocity	m/s
v_l	Liquid Velocity	m/s
V_{min}	Minimum air velocity	m/s
y	Boundary layer Height	m
δ	Boundary layer thickness	m
δ_ω	Vorticity thickness	m
$\lambda\perp$	Transversal wavelength	m
μ_g	Gas Dynamic Viscosity	kg/ms
μ_l	Liquid Dynamic Viscosity	kg/ms
ρ_g	Gas density (air)	kg/m^3
ρ_l	Liquid density (water)	kg/m^3
σ	Surface Tension	N/m

$C_f, = k_f / Re_{Air}^{0.2}$	Friction Coefficient
$M_x = \rho_g v_g^2 e_g / \rho_l v_l^2 e_l$	Momentum ratio
$M = \rho_g v_g^2 / \rho_g v_g^2 e_g$	Momentum flux ratio
$Re_{Air} = \rho_g v_g c_{inj} / \mu_g$	Air Reynolds number
$Re_{Water} = \rho_l v_l c_{inj} / \mu_l$	Water Reynolds number
$We = \rho_g v_g^2 c_{inj} / \sigma$	Webber Number

REFERENCES

[1] A. H. Lefebvre, Atomization and Sprays Lecture Notes, Lecture Notes, *Combustion an International Series, Norman Chigier Editor,* vol. 11, pp. 7, 1989.

[2] P. Berthoumieu, H.Carentz and A. Muller, Video techniques applied to the characterisation of liquid sheet break-up, 9th International Symposium on Flow Visualization, 2000.

[3] Chigier N. and C. Dumouchel, Atomization of Liquid Sheets, Prog. Astronaut Aeronaut, vol 166, pp241-259 1996.

[4] Choi. C. J. Choi and Lee S. Y., Droplet formation from a thing hollow Liquid Jet, 1960.

[5] Umesh Bhayaraju and Christoph Hassa, Surface Wave Propagartion And Breakup In Planar Liquid Sheets Of Prefilming Airblast Atomizers, *ICLASS-2006*.

[6] Feras Z. Batarseh, Ilia V. Roisman and Cameron Tropea, Effect Of Primary Spray Characteristics On The Spray Generated By An Airblast Atomizer Under High-Pressure Conditions, ILASS Americas, 2008

[7] I.S. Carvalho, M.V. Heitor and D. Santos, Liquid Film Disintegration Mechanisms, Third International Converence on Multiphase Flow, ICMFi98, Lyon, France, 1998.

[8] A. Lozano, F. Barreras, C. Siegler, D. Löw, The effects of Sheet Thickness on the oscillation of an air-blasted liquid Sheet, 2004

[9] Stapper B.E, Sowa W. A. And Samuelsen G. S., An Experimental Study of the Effects of Liquid Properties on the Break-up of a two-dimensional Liquid Sheet, Gas turbine and Aeroengine Congress and Exposition, 1990.

[10] Mansour A. and Chigier N. Dynamic Behaviour of liquid sheets, Phys. Fluids A 3 (12), 1991

[11] Lalo M., Atomization d'un film liquid mince par action combine des instabilities de Kelvin-Helmholtz et de Faraday: Application aux injecteurs aérodynamiques des turbomachies aéronautiques, These de l'Écoles nationales supérieure de l'aéronautique et de l'espace, ONERA Toulouse, 2006.

[12] B. E. Stapper and G. S. Samuelsen, An Experimental Study Of The Break-Up Of A Two-Dimensional Liquid Sheet In The Presence Of Co-Flow Air Shear, AIAA paper 90-0461, 1990.

[13] Hsiang L.-P. and Faeth G.M., drop deformation due to shock wave and steady disturbances, Int. J. Of Multiphase Flow, vol. 21 (4), pp 545-560, 1995

[14] Mansour A. and Chigier N. Disintegration of Liquid Sheets, Phys, Fluids A, vol 2 (5), pp.706-719, 1990

[15] Carentz H., Étude de la pulverisation d'une nappe liquid mince, These Universite Pierre et Marie Curie, 2000.

[16] Fraser R. P. and Eisenklam P., Research into the Performance of Atomizers for liquids, Imp. Coll. Chem. Eng. Soc. J., Vol. 7, 1953, pp. 52-68

[17] Larricq C., Etude de la pulverisation assistée en air d'une nappe liquid et influence d'un vent ionique sur les intabilités hydrodinamiques, PhD Thesis ONERA Toulouse, 2006.

[18] Lozano A., Félix Barreras, Guillermo Hauke and César Dopazo, Longitudinal Instabilities in a liquid sheet, J.Fluid Mech (2001), vol 437, pp 143-173, 2000.

[19] Yunus A. Çengel and John M. Cimbala, Fluid Dynamics Fundamentals and Applications, McGraw-Hill International Edition, pp. 530-531, 2006.

[20] Marmottant P., Villermaux Emmanuel, Fragmentation of stretched liquid ligaments, *Physics of Fluids vol 16 n°8 pp. 2732-2741*, 2004.